Evanescent waves in two-dimensional fluid-saturated porous metamaterials with a transversely isotropic matrix

Yan-Feng Wang,[1] Jun-Wei Liang,[2,*] A-Li Chen,[2] Yue-Sheng Wang,[1,†] and Vincent Laude[3,‡]
[1]*Department of Mechanics, School of Mechanical Engineering, Tianjin University, 300350 Tianjin, China*
[2]*Institute of Engineering Mechanics, Beijing Jiaotong University, 100044 Beijing, China*
[3]*Institut FEMTO-ST, Université Bourgogne Franche-Comté, CNRS, 25030 Besançon, France*

(Received 25 February 2020; revised manuscript received 30 March 2020; accepted 14 April 2020; published 1 May 2020)

Wave propagation in a two-dimensional periodic fluid-saturated porous metamaterial (FSPM) is investigated. The constitutive relation considered for fluid-saturated porous materials is based on Biot's homogeneization theory. Such media generally support two shear and two longitudinal elastic waves. Anisotropic wave propagation results both from anisotropy of the solid matrix and from the periodic structure of the metamaterial. Special attention is devoted to the dispersion and attenuation of evanescent Bloch waves in a FSPM whose matrix is transversely isotropic in which case in-plane elastic waves are a superposition of one shear wave and of two longitudinal waves. Bloch waves, complex band structures, and transmission properties are obtained numerically using finite element analysis. The case of homogeneous fluid-saturated porous media is considered since numerical simulations can be compared directly with analytic results in this case. The effects of material anisotropy and of fluid viscosity on wave propagation in two-dimensional FSPM are then discussed. It is found that wave-number band gaps appear in the complex band structure of the lossless FSPM due to the interference of waves with different but nonorthogonal polarizations. Wave-number band gaps are connected continuously by complex-frequency bands, hence, defining stop bands in the time domain. No complete frequency band gaps are found in two-dimensional lossless FSPM, in contrast to the one-dimensional case [Y.-F. Wang *et al.* Phys. Rev. B **99**, 134304 (2019)] due to the presence of the additional quasishear wave accompanying the two quasilongitudinal waves. Both the complex band structure and the transmission properties are affected by the anisotropy of the solid matrix. Wide transmission dips come up when viscosity is introduced as a result of the strong attenuation and the coupling of all wave polarizations. Concurrently, wave-number band gaps are washed out by viscosity. This theoretical paper has relevance to practical applications of fluid-saturated porous metamaterials, e.g., in concrete structures and geological soils.

DOI: 10.1103/PhysRevB.101.184301

I. INTRODUCTION

Phononic crystals (PCs) and acoustic metamaterials (AMs) are artificial composites which can alter efficiently the propagation of acoustic and elastic waves [1]. Phononic crystals are made of periodic inclusions embedded in a solid or fluid matrix [2]. They can influence significantly the dispersion of waves through Bragg scattering when the lattice constant is comparable with the wavelength. Acoustic metamaterials can further present the additional characteristics of local resonance [3]. They are, thus, less dependent on periodicity, and their operating wavelength can be much larger than their structural parameters. In this regime, they can then be considered as homogeneously effective media, presenting, in certain instances, negative effective mass density and/or modulus [4–6] and thereby leading to unusual wave functions. PCs and AMs have various potential applications in vibration reduction, wave rectification, negative refraction, cloaking, and more [7]. Tunable or active manipulation of waves can further be realized by mechanically changing the geometrical configuration or introducing multifield coupling components [8].

We note that most studies focus on PCs and AMs made of single-phase media, i.e., solids or fluids. Multiphase media, such as fluid-saturated porous (FSP) media [9,10] (made of a solid skeleton whose pores are saturated with a fluid), are, in contrast, less frequently considered. FSP media, however, offer further opportunities for the control of wave propagation [11–13]. In 1956, Biot presented a phenomenological homogeneization theory for wave propagation in two-phase FSP media [9,10] and suggested the existence of two longitudinal and two transverse waves, in contrast to elastic media that support only one longitudinal wave and two transverse waves. Later, the slow longitudinal wave was experimentally unveiled by Plona [14] and Dutta [15]. Researchers from different disciplines further discussed wave propagation in FSP media [16–21].

Elaborating upon the principles of phononic crystals and acoustic metamaterials, periodic inclusions can be introduced in FSP media to induce wave interference or resonance. For example, periodic wave barriers have received increasing

*Present address: China Railway Construction Investment Group Corporation Limited, 100044 Beijing, China.
†yswang@tju.edu.cn
‡vincent.laude@femto-st.fr

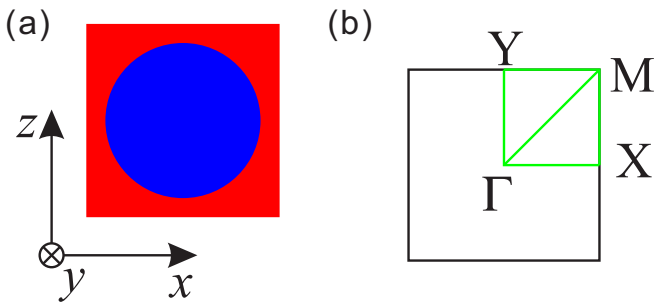

FIG. 1. Geometry definitions. (a) The unit cell of a two-dimensional (2D) square-lattice fluid-saturated porous metamaterial with cylindrical inclusions embedded in a transversely isotropic matrix is sketched. Both the inclusion and the matrix are composed of a FSP medium. The lattice constant is $a = 2$ m. Periodicity is on the (x, z) plane; the y direction is infinite. The principal axis of transversely isotropic media is the z axis. (b) The first Brillouin zone is also square, but high-symmetry points X and Y are nonequivalent because of anisotropy.

attention in order to reduce unwanted vibrations from traffic vehicles or seismic waves [22–26]. We note that natural soil was assumed to be single phase in most of these works. Although field experiments on seismic metamaterials were actually conducted [27–29], the accompanying models were limited to elastic waves. Some other works considered the metaporous material [16] composed of periodic inclusions [30,31], possibly including resonators [32]. Only acoustic properties, such as absorption or transmission, were, however, studied [32–35]. It was further noted that, in the submerged case, only one branch starts from the zero frequency and that the Γ point in either real and complex band structures [36], which is consistent with the fact that only longitudinal waves are incident from the surrounding fluid. This line of reasoning, however, does not apply if incidence is from a solid medium. Furthermore, the interference of the fast and the slow longitudinal waves can hardly be distinguished from such band structures.

Recently, we investigated wave propagation in one-dimensional (1D) fluid-saturated porous metamaterials (FSPMs) [37]. The term metamaterial is here chosen to emphasize applications in ground structuring and seismology [27]. We focused on some unique characteristics of waves in FSPMs: complex band structures for both the fast and the slow longitudinal waves and the avoided crossings between them. In the present paper, we extend our consideration to evanescent wave propagation in two-dimensional periodic FSPMs with a transversely isotropic matrix [38–40]. Under this setting, anisotropic wave propagation results both from the solid matrix and from the periodic structure of the metamaterial. As we discuss in this paper, differences with the one-dimensional case include the absence of complete frequency band gaps due to the presence of the additional quasishear wave accompanying the two quasilongitudinal waves, and the appearance of wave-number band gaps. In Sec. II, we discuss harmonic Bloch wave propagation and the implementation of adequate finite element methods (FEMs). Numerical results are given in Sec. III. We first compare the analytical and simulated results in the case of homogeneous FSP media for verification. The effects of material anisotropy and of viscosity on the complex band structure and the frequency response functions are then discussed. Finally, we summarize the main findings of the present paper and suggest some possible extensions.

II. HARMONIC BLOCH WAVE PROPAGATION

The geometry considered is depicted in Fig. 1. Note that periodicity is on the (x, z) plane but that the principal axis of transversely isotropic media is the z axis, i.e., transverse isotropy applies on the (x, y) plane. The basic equations derived from Biot's homogeneization theory are summarized in Appendix A. Biot equations for harmonic time dependency can be written in terms of either skeleton displacement and fluid displacement or skeleton displacement and fluid pressure [41]. In the one-dimensional case, both formulations are equivalent. In the present paper, we choose the latter form not only for its computational efficiency, but also to avoid the appearance of null eigenvalues as we explain below.

A. Harmonic waves

The skeleton displacements are u_i with $i = 1 \cdots 3$, and the fluid pressure in the pores is p. The four independent variables u_i and p are grouped in a state vector,

$$[u_i, p] = [\bar{u}_i, \bar{p}]e^{-\imath\omega t}, \tag{1}$$

where t is the time variable, ω is the angular frequency, and $\bar{u}_i$ and $\bar{p}$ are periodic functions of position otherwise independent of time.

The governing wave equations can be obtained by combining the constitutive and dynamic equations (A2) and (A4),

$$\begin{aligned}
&B_9\frac{\partial^2\bar{u}_x}{\partial x^2} + B_1\frac{\partial^2\bar{u}_x}{\partial y^2} + B_5\frac{\partial^2\bar{u}_x}{\partial z^2} + (B_9 - B_1)\frac{\partial^2\bar{u}_y}{\partial x\,\partial y} + B_{10}\frac{\partial^2\bar{u}_z}{\partial x\,\partial z} + \left(\frac{B_6}{B_8} + \frac{\rho_f}{\bar{m}_1}\right)\frac{\partial\bar{p}}{\partial x} + \left(\rho - \frac{\rho_f^2}{\bar{m}_1}\right)\omega^2\bar{u}_x = 0,\\
&(B_9 - B_1)\frac{\partial^2\bar{u}_x}{\partial x\,\partial y} + B_1\frac{\partial^2\bar{u}_y}{\partial x^2} + B_9\frac{\partial^2\bar{u}_y}{\partial y^2} + B_5\frac{\partial^2\bar{u}_y}{\partial z^2} + B_{10}\frac{\partial^2\bar{u}_z}{\partial y\,\partial z} + \left(\frac{B_6}{B_8} + \frac{\rho_f}{\bar{m}_2}\right)\frac{\partial\bar{p}}{\partial y} + \left(\rho - \frac{\rho_f^2}{\bar{m}_2}\right)\omega^2\bar{u}_y = 0,\\
&B_{10}\frac{\partial^2\bar{u}_x}{\partial x\,\partial z} + B_{10}\frac{\partial^2\bar{u}_y}{\partial y\,\partial z} + B_5\frac{\partial^2\bar{u}_z}{\partial x^2} + B_5\frac{\partial^2\bar{u}_z}{\partial y^2} + \left(B_4 - B_7^2/B_8\right)\frac{\partial^2\bar{u}_z}{\partial z^2} + \left(\frac{B_7}{B_8} + \frac{\rho_f}{\bar{m}_3}\right)\frac{\partial\bar{p}}{\partial z} + \left(\rho - \frac{\rho_f^2}{\bar{m}_3}\right)\omega^2\bar{u}_z = 0,\\
&-\left(\frac{B_6}{B_8} + \frac{\rho_f}{\bar{m}_1}\right)\frac{\partial\bar{u}_x}{\partial x} - \left(\frac{B_6}{B_8} + \frac{\rho_f}{\bar{m}_2}\right)\frac{\partial\bar{u}_y}{\partial y} - \left(\frac{B_7}{B_8} + \frac{\rho_f}{\bar{m}_3}\right)\frac{\partial\bar{u}_z}{\partial z} + \frac{1}{\bar{m}_1\omega^2}\frac{\partial^2\bar{p}}{\partial x^2} + \frac{1}{\bar{m}_2\omega^2}\frac{\partial^2\bar{p}}{\partial y^2} + \frac{1}{\bar{m}_3\omega^2}\frac{\partial^2\bar{p}}{\partial z^2} + \frac{1}{B_8}\bar{p} = 0,
\end{aligned} \tag{2}$$

with $B_9 = (2B_1 + B_2 - \frac{B_6^2}{B_8})$, $B_{10} = (B_3 + B_5 - \frac{B_6 B_7}{B_8})$, and $\bar{m}_i = m_i + \imath r_i/\omega$. The expressions of the various coefficients are given in Appendix A. Since we will examine the effect of material anisotropy on wave propagation, we suppose that propagation is on the x-z plane. Then, modes of propagation decouple into in-plane and out-of-plane modes. For in-plane modes, we have three coupled equations,

$$
\begin{aligned}
&B_9\frac{\partial^2\bar{u}_x}{\partial x^2} + B_5\frac{\partial^2\bar{u}_x}{\partial z^2} + B_{10}\frac{\partial^2\bar{u}_z}{\partial x\,\partial z} + \left(\frac{B_6}{B_8} + \frac{\rho_f}{\bar{m}_1}\right)\frac{\partial\bar{p}}{\partial x} + \left(\rho - \frac{\rho_f^2}{\bar{m}_1}\right)\omega^2\bar{u}_x = 0,\\
&B_{10}\frac{\partial^2\bar{u}_x}{\partial x\,\partial z} + B_5\frac{\partial^2\bar{u}_z}{\partial x^2} + \left(B_4 - B_7^2/B_8\right)\frac{\partial^2\bar{u}_z}{\partial z^2} + \left(\frac{B_7}{B_8} + \frac{\rho_f}{\bar{m}_3}\right)\frac{\partial\bar{p}}{\partial z} + \left(\rho - \frac{\rho_f^2}{\bar{m}_3}\right)\omega^2\bar{u}_z = 0,\\
&-\left(\frac{B_6}{B_8} + \frac{\rho_f}{\bar{m}_1}\right)\frac{\partial\bar{u}_x}{\partial x} - \left(\frac{B_7}{B_8} + \frac{\rho_f}{\bar{m}_3}\right)\frac{\partial\bar{u}_z}{\partial z} + \frac{1}{\bar{m}_1\omega^2}\frac{\partial^2\bar{p}}{\partial x^2} + \frac{1}{\bar{m}_3\omega^2}\frac{\partial^2\bar{p}}{\partial z^2} + \frac{1}{B_8}\bar{p} = 0,
\end{aligned}
\tag{3}
$$

whereas we have a scalar equation for out-of-plane modes,

$$
B_1\frac{\partial^2\bar{u}_y}{\partial x^2} + B_5\frac{\partial^2\bar{u}_y}{\partial z^2} + \left(\rho - \frac{\rho_f^2}{\bar{m}_2}\right)\omega^2\bar{u}_y = 0. \tag{4}
$$

Equation (4) is independent of the fluid pressure and is similar to the equation for vertical shear waves propagating in a single phase (homogenized) elastic medium. In the following, we, thus, limit our discussion to in-plane modes described by Eq. (3) with the three degrees of freedom $(\bar{u}_x, \bar{u}_z, \bar{p})$. Note that the mixed system of equations does not possess a particular symmetry.

B. Bloch waves

According to Bloch's theorem, the displacement field for eigenmodes of the periodic medium can be written

$$
[\bar{u}_x, \bar{u}_z, \bar{p}] = [\tilde{u}_x, \tilde{u}_z, \tilde{p}]e^{\imath k(l_1 x + l_3 z)}, \tag{5}
$$

where $\tilde{u}_x$, $\tilde{u}_z$, and $\tilde{p}$ are amplitudes as a function of the position and k is the wave number whose real part can be restricted to the irreducible Brillouin zone of the reciprocal lattice. Suppose the angle between the propagation direction and the x axis is θ, then, the direction of propagation is given by $l_1 = \cos\theta$ and $l_3 = \sin\theta$. Substituting Eq. (5) into Eq. (3), we get the system of equations,

$$
\begin{aligned}
&B_9\frac{\partial^2\tilde{u}_x}{\partial x^2} + B_5\frac{\partial^2\tilde{u}_x}{\partial z^2} + B_{10}\frac{\partial^2\tilde{u}_z}{\partial x\,\partial z} + 2\imath k l_1 B_9\frac{\partial\tilde{u}_x}{\partial x} + 2\imath k l_3 B_5\frac{\partial\tilde{u}_x}{\partial z} + \imath k l_3 B_{10}\frac{\partial\tilde{u}_z}{\partial x} + \imath k l_1 B_{10}\frac{\partial\tilde{u}_z}{\partial z}\\
&\quad - \left(B_9 k^2 l_1^2 + B_5 k^2 l_3^2\right)\tilde{u}_x - B_{10}k^2 l_1 l_3\tilde{u}_z + \left(\frac{B_6}{B_8} + \frac{\rho_f}{\bar{m}_1}\right)\frac{\partial\tilde{p}}{\partial x} + \imath k l_1\left(\frac{B_6}{B_8} + \frac{\rho_f}{\bar{m}_1}\right)\tilde{p} + \left(\rho - \frac{\rho_f^2}{\bar{m}_1}\right)\omega^2\tilde{u}_x = 0,\\
&B_{10}\frac{\partial^2\tilde{u}_x}{\partial x\,\partial z} + B_5\frac{\partial^2\tilde{u}_z}{\partial x^2} + \left(B_4 - \frac{B_7^2}{B_8}\right)\frac{\partial^2\tilde{u}_z}{\partial z^2} + \imath k l_3 B_{10}\frac{\partial\tilde{u}_x}{\partial x} + \imath k l_1 B_{10}\frac{\partial\tilde{u}_x}{\partial z} + 2\imath k l_1 B_5\frac{\partial\tilde{u}_z}{\partial x} + 2\imath k l_3\left(B_4 - \frac{B_7^2}{B_8}\right)\frac{\partial\tilde{u}_z}{\partial z}\\
&\quad - \left[\left(B_4 - \frac{B_7^2}{B_8}\right)k^2 l_3^2 + B_5 k^2 l_1^2\right]\tilde{u}_z - B_{10}k^2 l_1 l_3\tilde{u}_x + \left(\frac{B_7}{B_8} + \frac{\rho_f}{\bar{m}_3}\right)\frac{\partial\tilde{p}}{\partial z} + \imath k l_3\left(\frac{B_7}{B_8} + \frac{\rho_f}{\bar{m}_3}\right)\tilde{p} + \left(\rho - \frac{\rho_f^2}{\bar{m}_3}\right)\omega^2\tilde{u}_z = 0,\\
&-\left(\frac{B_6}{B_8} + \frac{\rho_f}{\bar{m}_1}\right)\frac{\partial\tilde{u}_x}{\partial x} - \left(\frac{B_7}{B_8} + \frac{\rho_f}{\bar{m}_3}\right)\frac{\partial\tilde{u}_z}{\partial z} - \imath k_1\left(\frac{B_6}{B_8} + \frac{\rho_f}{\bar{m}_1}\right)\tilde{u}_x - \imath k l_3\left(\frac{B_7}{B_8} + \frac{\rho_f}{\bar{m}_3}\right)\tilde{u}_z\\
&\quad + \frac{1}{\bar{m}_1\omega^2}\frac{\partial^2\tilde{p}}{\partial x^2} + \frac{1}{\bar{m}_3\omega^2}\frac{\partial^2\tilde{p}}{\partial z^2} + \frac{2\imath k_1}{\bar{m}_1\omega^2}\frac{\partial\tilde{p}}{\partial x} + \frac{2\imath k l_3}{\bar{m}_3\omega^2}\frac{\partial\tilde{p}}{\partial z} + \left(\frac{1}{B_8} - \frac{k^2 l_1^2}{\bar{m}_1\omega^2} - \frac{k^2 l_3^2}{\bar{m}_3\omega^2}\right)\tilde{p} = 0.x
\end{aligned}
\tag{6}
$$

Note that the last equation can also be multiplied by ω^2 to produce a form suitable for eigenvalue problems.

For inhomogeneous FSPMs with periodic inclusions, such as depicted in Fig. 1, Eq. (7) can be solved by the finite element method. At the interface between the inclusions and the matrix, the pores are chosen to be open [42], and the field variables $\mathbf{u} = (\tilde{u}_x, \tilde{u}_z, \tilde{p})$ are continuous [41]. We write the coefficient form of the resulting equation, suitable for use with the partial differential equation module of COMSOL MULTIPHYSICS, for instance [5], as

$$
\lambda^2 A_1\mathbf{u} - \lambda A_2\mathbf{u} - \nabla\cdot(A_0{:}\nabla\mathbf{u} + A_3\mathbf{u}) + A_4\nabla\mathbf{u} + A_5\mathbf{u} = 0, \tag{7}
$$

where $\lambda = \imath k$ and the coefficient matrices are listed in Appendix B. Since the dynamic material parameters of FSP media are frequency dependent, band structures with complex wave numbers [5,43] are the first choice for the analysis. For

this purpose, we set the eigenvalue as $\lambda = \imath k$. Complex-wavenumber band structures are then obtained by sweeping ω in the frequency range of interest.

In particular, if the pore fluid is lossless, i.e., if the viscosity $\eta = 0$, or if the permeability is infinite, i.e., $K(0) \to \infty$, we have $m = \alpha(\infty)\rho_f/\phi$ nondispersive and $r = 0$ identically. Equation (7) can then be solved for the band structure with complex frequency and real wave number by choosing the eigenvalue as $\lambda = \imath\omega$. It still, however, involves frequency-dependent coefficients and, thus, produces a nonlinear generalized eigenvalue problem. The coefficient matrices appearing in Eq. (7) are then listed in Appendix C. The complex-frequency band structure is obtained in practice by sweeping k inside the first Brillouin zone of the 2D square lattice.

For comparison with the different band structures, we can also calculate the frequency response function (FRF) [44] of a finite system by solving directly Eq. (3). The nonzero coefficient matrices are listed in Appendix D. Harmonic excitation with unit amplitude is applied to the left side (with area S_l) of the finite system. Polarizations $(\bar{u}_x, \bar{u}_z, \bar{p}) = (1, 0, 0)$, (0,1,0) or (0,0,1) are considered as excitations. Harmonic responses are measured on the right side (with area S_r) of the system, and the frequency response function is defined as

$$\mathrm{FRF} = \frac{\int \sqrt{\bar{u}_x^2 + \bar{u}_z^2 + \bar{w}_x^2 + \bar{w}_z^2}\, dS_r}{\int \sqrt{\bar{u}_x^2 + \bar{u}_z^2 + \bar{w}_x^2 + \bar{w}_z^2}\, dS_l}, \tag{8}$$

where the fluid displacements are derived from Eq. (A4) as $\bar{w}_x = (\partial\bar{p}/\partial x - \rho_f\omega^2\bar{u}_x)/\bar{m}_1/\omega^2$ and $\bar{w}_z = (\partial\bar{p}/\partial z - \rho_f\omega^2\bar{u}_z)/\bar{m}_3/\omega^2$.

C. Homogeneous fluid-saturated porous media

For homogeneous FSP media, the amplitudes $\tilde{u}_x$, $\tilde{u}_z$, and $\tilde{p}$ are constants, so the partial derivative terms in Eq. (7) vanish. Then, Eq. (7) simplifies to

$$\begin{bmatrix} d_{11} & d_{12} & d_{13} \\ d_{21} & d_{22} & d_{23} \\ d_{31} & d_{32} & d_{33} \end{bmatrix} \begin{pmatrix} \tilde{u}_x \\ \tilde{u}_z \\ \tilde{p} \end{pmatrix} = 0, \tag{9}$$

where

$$d_{11} = \left(\rho - \frac{\rho_f^2}{m_1}\right)\omega^2 - \left(2B_1 + B_2 - \frac{B_6^2}{B_8}\right)k^2 l_1^2 - B_5 k^2 l_3^2,$$

$$d_{12} = d_{21} = -\left(B_3 + B_5 - \frac{B_6 B_7}{B_8}\right)k^2 l_1 l_3 - B_5 k^2 l_3^2,$$

$$d_{22} = \left(\rho - \frac{\rho_f^2}{m_3}\right)\omega^2 - B_5 k^2 l_1^2 - \left(B_4 - \frac{B_7^2}{B_8}\right)k^2 l_3^2,$$

$$d_{13} = -d_{31} = \left(\frac{\rho_f}{m_1} + \frac{B_6}{B_8}\right)\imath k l_1,$$

$$d_{23} = -d_{32} = \left(\frac{\rho_f}{m_3} + \frac{B_7}{B_8}\right)\imath k l_3,$$

$$d_{33} = \frac{1}{B_8} - \frac{k^2 l_1^2}{m_1\omega^2} - \frac{k^2 l_3^2}{m_3\omega^2}.$$

For Eq. (9) to have solutions for nonvanishing $\tilde{u}_x$, $\tilde{u}_z$, and $\tilde{p}$, we must have

$$\begin{vmatrix} d_{11} & d_{12} & d_{13} \\ d_{21} & d_{22} & d_{23} \\ d_{31} & d_{32} & d_{33} \end{vmatrix} = 0. \tag{10}$$

The above equation can be written as the cubic polynomial equation in k^2,

$$bk^6 + c\omega^2 k^4 + d\omega^4 k^2 + e\omega^6 = 0, \tag{11}$$

where coefficients b, c, d, and e are explicitly given in Appendix E. Denoting

$$\lambda = \frac{k^2}{\omega^2} + \frac{c}{3b}, \quad p = \frac{d}{b} + \frac{c^2}{3b^2}, \quad q = \frac{e}{b} + \frac{2c^3}{27b^3} - \frac{cd}{3b^2}, \tag{12}$$

Eq. (11) simplifies to

$$\lambda^3 + p\lambda + q = 0. \tag{13}$$

The three roots are

$$\lambda_1 = R_1 + R_2, \quad \lambda_2 = \gamma R_1 + \gamma^2 R_2, \quad \lambda_3 = \gamma^2 R_1 + \gamma R_2, \tag{14}$$

where

$$R_1 = \left(-\frac{q}{w} + \sqrt{\Xi}\right)^{1/3}, \quad R_2 = \left(-\frac{q}{w} - \sqrt{\Xi}\right)^{1/3},$$
$$\Xi = \left(\frac{q}{2}\right)^2 + \left(\frac{p}{3}\right)^3, \quad \gamma = \frac{-1 + \imath\sqrt{3}}{3}. \tag{15}$$

According to Eq. (13), the dispersion relation is then obtained as the three branches,

$$k_j = \omega\sqrt{\lambda_j - \frac{c}{3b}}, \quad j = 1\text{–}3. \tag{16}$$

Since the coefficients in Eq. (11) are complex, the single-valued complex branches of R_1 and R_2 should be carefully selected. Equation (16) also suggests that there are three different waves in the porous medium. For the isotropic case, these are the $P1$ (fast longitudinal) wave, the $P2$ (slow longitudinal) wave, and the shear vertical, or transverse (SV) wave. For the transversely isotropic case, these are the fast quasilongitudinal (QP1) wave, the slow quasilongitudinal (QP2) wave, and the quasishear vertical (QSV) wave. It is noted that the same solutions are obtained if fluid displacement is used in Biot's wave equation instead of pressure. In this case, however, Eq. (11) will be a quartic equation in k^2 with one zero root as we have checked. This occurs because the fluid pressure is replaced by two fluid displacement components so there is one spurious degree of freedom.

III. RESULTS AND DISCUSSION

In this section, Bloch wave propagation in 2D periodic FSPMs in a transversely isotropic matrix is investigated. Complex band structures and harmonic responses are given for different FSPMs composed from the materials listed in Table I. In order to obtain a convergent result for finite element computations, the smallest element of the mesh is chosen 50 times smaller than the lattice constant for the calculation

TABLE I. Independent material parameters of the fluid-saturated media considered in this paper.

Material parameters Units	ρ_s (kg/m^3)	ρ_f kg/m^3	C_{11} (GPa)	C_{12} (GPa)	C_{66} (GPa)	C_{33} (GPa)	C_{13} (GPa)	C_{44} (GPa)	K_s (GPa)	K_f (GPa)	$K_1(0)$ (Darcy)	$K_3(0)$ (Darcy)	$\alpha(\infty)$	ϕ
Transversely isotropic FSP medium	3000	1000	10	2	4	8	2.4	3.2	30	2	1	0.1	1	0.2
Isotropic FSP medium 1	3000	1000	10	2	4				30	2	1	1	1	0.2
Isotropic FSP medium 2 (steel)	7800	1000	171	41	65				96.17	2	1	1	1	0.01

of complex band structures and 20 times smaller for the calculation of frequency responses. Before moving to two-dimensional FSPMs, results are first presented for a homogeneous transversely isotropic FSP medium for reference and comparison.

A. Homogeneous transversely isotropic fluid-saturated porous media

We first consider the case of a homogeneous transversely isotropic FSP medium. Material parameters (similar to those used for sandrock [45]) are presented in the second line of Table I and the viscosity is set as $\eta = 1$ mPa s. The dispersion relation, or complex band structure with complex wavenumber $k(\omega)$ is plotted in Fig. 2 for wave propagation in directions $\theta = 0^\circ$ (ΓX), 45° (ΓM), and 90° (ΓY). The color scale represents the relative energy ratio of the kinetic-energy E_k^f in the pore fluid to the total kinetic energy and is defined as

$$\frac{\int e_k^f dS}{\int \left(e_k^s + e_k^f\right) dS}, \tag{17}$$

where S is the integration area of the unit cell, the kinetic energy in the solid skeleton is $e_k^s = (1-\phi)\rho_s\omega^2(u_x^2 + u_z^2)/2$, and $e_k^f = \phi\rho_f\omega^2(U_x^2 + U_z^2)/2$. Owing to the viscosity of the pore fluid, all three waves are dispersive and dissipative. The

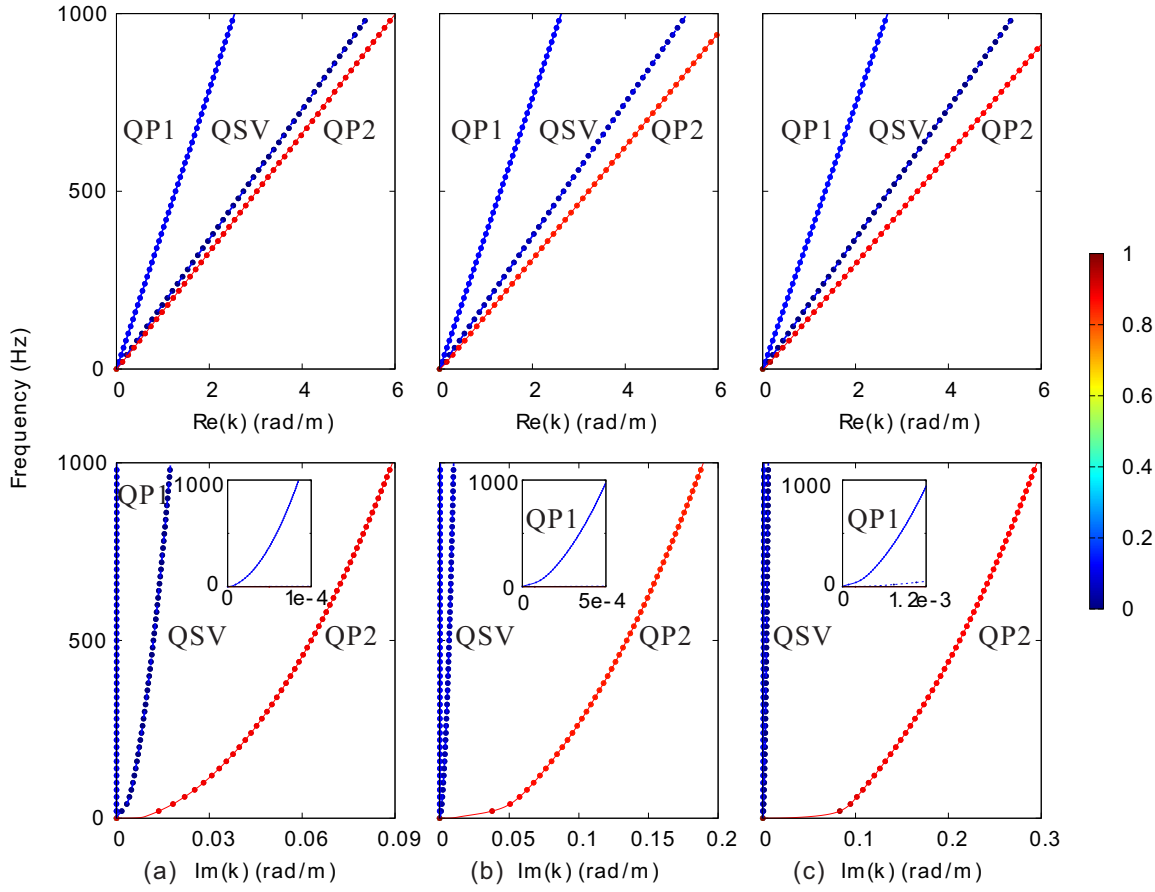

FIG. 2. Complex dispersion relation, or band structure, for a homogeneous transversely isotropic FSP medium for (a) $\theta = 0^\circ$, (b) 45°, and (c) 90°. The top and bottom panels illustrate the variation of frequency with the real and imaginary parts of the wave vector, respectively. The blue-solid, blue-dashed, and red-solid lines are for QP1, QSV, and QP2 waves of the analytical results of Eq. (16). The color scale measures the relative energy ratio between the pore fluid (1) and the solid skeleton (0). The insets shows a zoom of the imaginary part near the origin of the graphs.

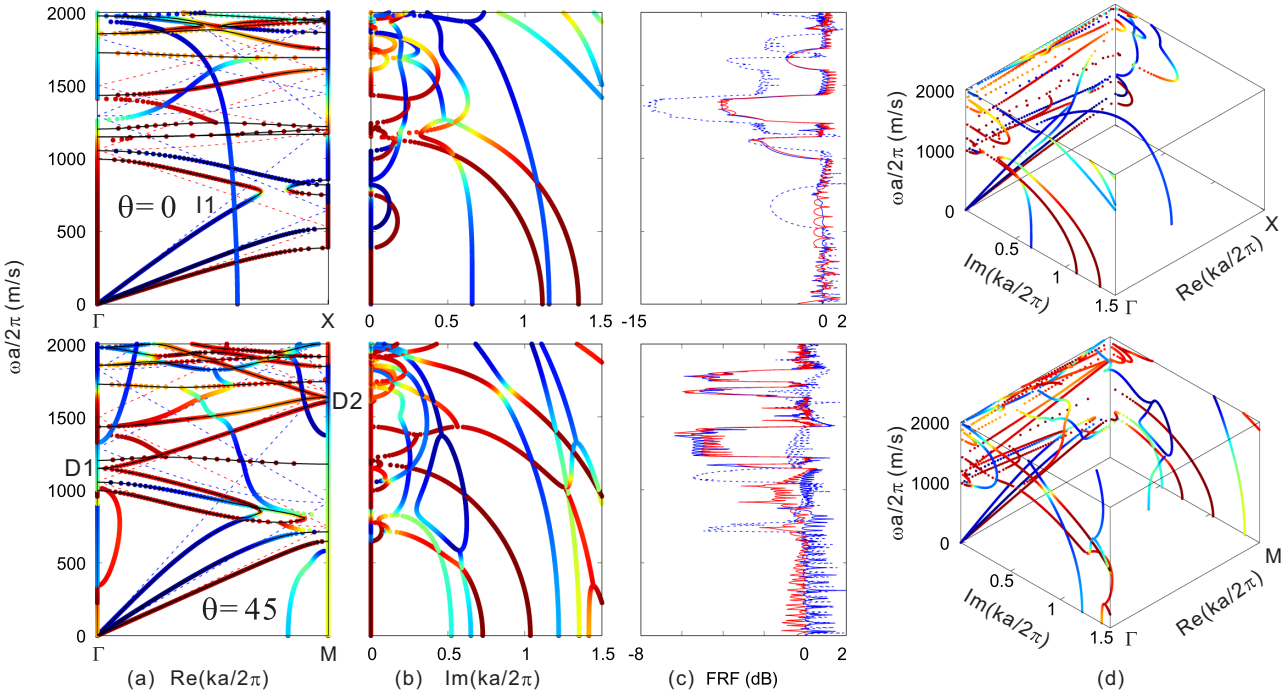

FIG. 3. Complex band structures for 2D lossless FSPM with periodic inclusions in an isotropic matrix for $\theta = 0^\circ$ and 45°. Panels (a) and (b) illustrate the variation of the frequency with the real and imaginary parts of the wave vector, respectively. The solid lines represent the real band structures calculated by FEM. The color scale indicates the relative energy ratio between the pore fluid (1) and the solid skeleton (0). Panel (c) shows the frequency response function of a finite system with the length of 40 unit cells for $\theta = 0^\circ$ and 14 unit cells for $\theta = 45^\circ$. The blue solid, blue dashed, and red solid lines represent the results for the excitation of $(\bar{u}_x, \bar{u}_z, \bar{p})$, respectively. Panels (d) show the same information as the complex band structures in (a) and (b) but plotted in a three-dimensional representation preserving the continuity of complex bands.

analytical result of Eq. (16) agrees exactly with the numerical simulation.

In the frequency range of interest, the real part of the wave number has a mostly linear dispersion. The imaginary part of the wave number generally increases quadratically with frequency, but its value for the QP2 wave is the largest, and that for the QP1 wave is the smallest. This indicates that attenuation is generally largest for the QP2 wave and that it is larger for the QSV wave compared to the QP1 wave.

It can further be noted that the imaginary part of the wave number for $\theta = 0^\circ$ is smaller than that for $\theta = 90^\circ$ as a direct consequence of material anisotropy. Indeed, since $C_{33} < C_{11}$, the rigidity of the medium is smaller in the latter case whereas viscosity remains isotropic, leading to an overall smaller wavelength (the real part of the inverse of k) and, hence, to larger spatial decay at constant temporal damping.

B. Lattice anisotropy

We now turn our attention to wave propagation in a 2D FSPM composed of cylindrical inclusions in a matrix arranged periodically according to a square lattice. In this section, we consider the effect of periodicity on waves propagating in-plane, disregarding first material anisotropy and viscosity. Both the inclusion and the matrix are isotropic FSP media. High-symmetry points X and Y of the first Brillouin zone are equivalent in this case. Material parameters for the matrix and the inclusion are listed in the third and fourth rows of Table I, respectively. The ratio between the radius of the inclusion and the lattice constant is 0.4. The complex band structures in Figs. 3(a), 3(b), and 3(d) show reduced frequency $\Omega = \omega a/(2\pi)$ as a function of reduced wave-number $ka/(2\pi)$ with a as the lattice constant. The result for an empty lattice (inclusions with vanishing radius) is also plotted with dashed lines for comparison. The frequency response functions in Fig. 3(c) are computed for a metamaterial thickness of $14a$ in the ΓX direction ($\theta = 0^\circ$), and $14\sqrt{2}a$ in the ΓM direction ($\theta = 45^\circ$).

In the complex band structures, three bands start at the Γ point and zero frequency, corresponding to waves QP1, QSV, and QP2 in the homogeneization limit. As frequency increases, these waves are coupled by the periodic microstructure and can hybridize. The complex band structures, hence, contain many complex bands $k(\omega)$ with mixed polarization. Several directional band gaps appear for propagation direction $\theta = 0^\circ$. When $\theta = 45^\circ$, the directional band gaps only exist for particular polarization modes. As a whole, no complete band gaps are observed. We checked that for a phononic crystal composed of elastic materials having the elastic constants listed in Table I and the same geometrical dimensions as the FSP crystal, complete band gaps would be found. The closure of the complete band gaps results from the appearance of the $P2$ wave that does not exist in purely elastic metamaterials.

Of particular interest is the avoided crossing appearing at the intersection of the bands supporting QP1 and QP2 waves

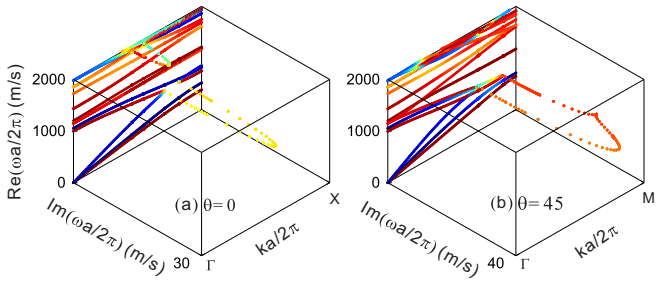

FIG. 4. Complex-frequency band structure of the lossless FSPM in the isotropic matrix in Fig. 3 for (a) $\theta = 0^\circ$ and (b) 45°. The color scale indicates the relative energy ratio between the pore fluid (1) and the solid skeleton (0).

as marked by point $I1$ in Fig. 3(a). As we observed previously for 1D FSPMs [37], the avoided crossing appears when periodicity introduces band folding. Unlike the vertical split at the degeneration point in 1D FSPMs, however, a horizontal split of the bands is observed here. A wave-number band gap [46] is, thus, formed inside the Brillouin zone for direction $\theta = 0^\circ$. For direction $\theta = 45^\circ$, two wave-number band gaps overlap near the high-symmetry point M, one for the QP1 and QP2 waves and the second for the QP2 and QSV waves. It has been noted that wave-number band gaps could appear in single-phase metamaterials when the dispersion curve is cut off under a relatively high general damping [46]. In the present case, viscosity is neglected and damping is not at stake. As a result, it is the introduction of the pore fluid, and, more precisely, the interference of the two longitudinal waves, that gives rise to wave-number band gaps. Of course, periodicity is also essential since a band folding is involved. As a note, such wave-number band gaps do not show up for a 1D FSPM [37] nor in the homogeneous case.

Looking at the representation of the complex band structures of Fig. 3(d), there are no evanescent branches connecting the two sides of the wave-number band gaps. This is in marked contrast with Bragg and locally resonant band gaps for which a complex evanescent branch always connects the bands at the entrance and at the exit of the frequency band gap [5,43]. As a matter of fact, continuity through the wave-number band gap is provided by a complex-frequency branch rather than a complex-wave-number branch. In order to sustain this assertion, we present, in Fig. 4, the complex-frequency band structure for the FSPM of Fig. 3. The complex-frequency band structure [47] is obtained by solving for complex ω as a function of real k, as we outlined in Sec. III B. It can be seen in Fig. 4 that the frequency becomes complex inside wave-number band gaps. For direction $\theta = 0^\circ$, a complex-frequency branch connects the entrance and exit of the wave-number band gap horizontally, i.e., at fixed real k inside the first Brillouin zone. For direction $\theta = 45^\circ$, the continuous connecting complex branches involve a mixture of QP1, QP2, and QSV waves. In either case, waves of a given frequency are damped in time when their wave number falls within a specific interval.

C. Material anisotropy

Next, we introduce material anisotropy by replacing, in the matrix, the isotropic FSP medium by the transversely isotropic FSP medium whose material properties are listed in the second row of Table I. The isotropic inclusions are unchanged compared to Sec. III B. Complex band structures for directions $\theta = 0^\circ$ (ΓX), 45° (ΓM), and 90° (ΓY) are shown in Fig. 5.

Comparing with Fig. 3, the main difference is that high-symmetry points X and Y are now nonequivalent. As the rigidities of the transversely isotropic FSP medium have been chosen as slightly smaller than those of the isotropic FSP medium, most bands generally shift downward in frequency and especially the QP2 bands. Because there is less symmetry in the elastic tensor, bands that were degenerated at points $D1$ and $D2$ now give rise to small directional band gaps in ranges of $1095.5 < \Omega < 1137.8$ and $1577.4 < \Omega < 1623.7$ m/s. Thus, a complete band gap is now found in the range of $1597.4 < \Omega < 1623.7$ m/s. Wave-number band gaps are still present, and the wave-number band gap for direction $\theta = 45^\circ$ is apparently enlarged. Surprisingly, the transmission does not change too much between directions $\theta = 0^\circ$ and $\theta = 90^\circ$ but becomes larger for direction $\theta = 45^\circ$ as if the directional band gaps were closed by the presence of shifted bands.

D. Fluid viscosity

In this section, we consider 2D periodic FSPMs with a transversely isotropic matrix with nonzero viscosity. As a note, only evanescent waves exist in the viscous case. Results are summarized in Fig. 6 for direction $\theta = 0^\circ$ and in Fig. 7 for direction $\theta = 45^\circ$.

The complex band structures are already strongly affected when even a small viscosity ($\eta = 10^{-7}$ Pa s) is introduced, see Fig. 6. As usual, when loss is introduced [48], the sharp corners of bands at the high-symmetry points of the Brillouin zone become rounded. This rounding effect is especially marked for longitudinal waves since they are intrinsically more sensitive to longitudinal viscosity. Shear waves are, however, also sensitive to the viscosity of fluid as the 2D structuration of the matrix couples shear and longitudinal strains in the metamaterial.

The wave-number band gap is still present for direction $\theta = 0^\circ$. For direction $\theta = 45^\circ$, in contrast, the wave-number band gap is hardly observable due to the reconstruction of the dispersion bands caused by viscosity. Various fully complex-valued bands appear starting from the zero frequency. It can, indeed, be seen, in Fig. 6(d), that all bands move inside the complex wave-number plane: There are no more purely real bands for lossless transmission and no more purely imaginary bands describing usual frequency band gaps. It is also observed, in Figs. 6 and 7, that the imaginary part of the wave number of the QP2 wave is more affected by fluid viscosity than that of the QP1 and QSV waves.

The frequency response function for direction $\theta = 0^\circ$ becomes smoother, assuming smaller values in the initially passing bands but larger values inside frequency band gaps. The lowest band gap for shear waves is less affected since viscous loss is smaller for them compared to longitudinal

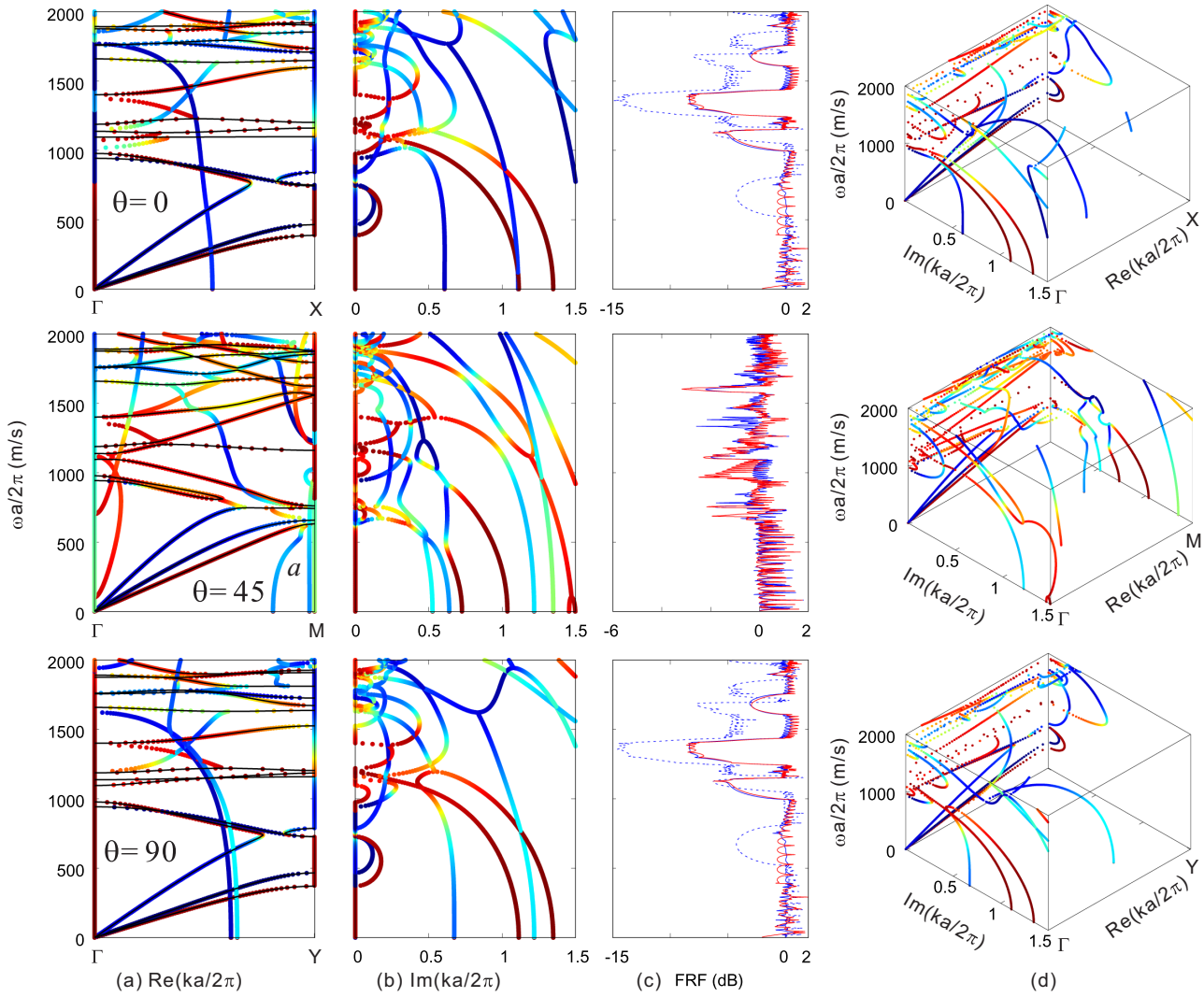

FIG. 5. Complex band structures for 2D lossless periodic FSPM in transversely isotropic matrix for $\theta = 0^\circ$, 45°, and 90°. Panels (a) and (b) illustrate the variation of the frequency with the real and imaginary parts of the wave vector, respectively. The solid lines represent for the real band structures calculated by FEM. The color scale indicates the relative energy ratio between the pore fluid (1) and the solid skeleton (0). Panel (c) shows the frequency response function of a finite system with the length of 40 unit cells for $\theta = 0^\circ$ and 90° and 14 unit cells for $\theta = 45^\circ$. The blue solid, blue dashed, and red solid lines represent the results for the excitation of $(\bar{u}_x, \bar{u}_z, \bar{p})$, respectively.

waves. For direction $\theta = 45^\circ$, the transmission generally gets much smaller than in the absence of viscosity for frequencies above the first band gaps. The directional band gaps merge, leading to an apparent much larger complete band gap.

Similar trends are observed when viscosity is increased to $\eta = 10^{-5}$ Pa s in Fig. 7. As apparent in Fig. 7(d), the bands occupy more and more of the available complex wave-number space. Wave-number band gaps are still present for direction $\theta = 0^\circ$. The transmission dip frequency responses become even smoother and deeper, defining clear attenuation band gaps. This effect is particularly marked for direction $\theta = 45^\circ$.

We further checked that the effects of fluid viscosity on the complex band structure and on transmission in the ΓY direction are similar to those in the ΓX direction. The values of transmission are quite different for directions ΓM and $\Gamma X(Y)$ when fluid viscosity is zero (such as in Figs. 3 and 5) or is small (such as for $\eta = 10^{-7}$ Pa s in Figs. 6 and 7). Such an imbalance is generally not observed in periodic systems with single-phase materials. However, it almost disappears for larger viscosity (i.e., for $\eta = 10^{-5}$ Pa s in Figs. 6 and 7).

IV. CONCLUSIONS

In this paper, wave propagation in 2D periodic FSPMs with an isotropic or a transversely isotropic matrix has been investigated comprehensively. Such metamaterials support a total of four modes of propagation with two longitudinal waves and two shear waves, three of them being coupled by the anisotropy of the 2D microstructure. The finite element method was used to calculate band structures with either complex wave number or complex frequency, and the frequency response (transmission) of finite-thickness FSP metamaterials. For verification, the dispersion relation for homogeneous transversely isotropic FSP media was analyzed theoretically. Numerical and theoretical results are entirely consistent in the homogeneous case. It is observed that wave-number band

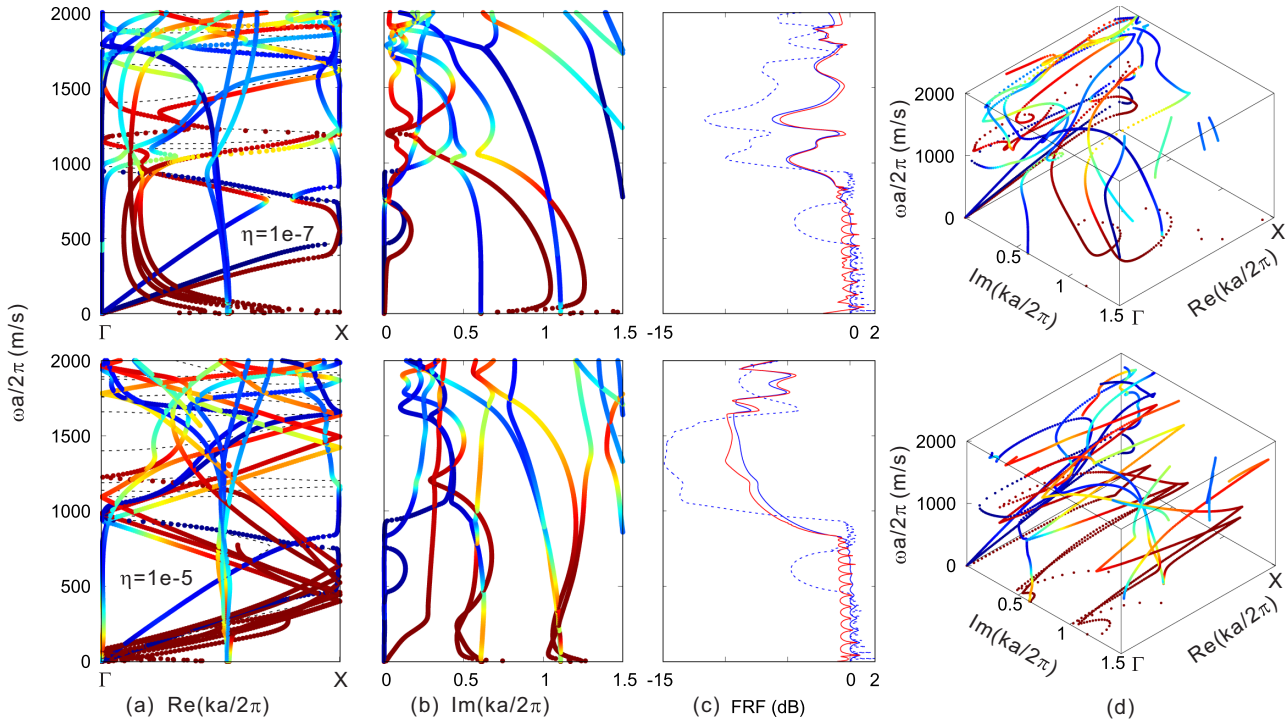

FIG. 6. Effects of fluid viscosity on the complex band structures and transmission spectrum of 2D periodic FSPMs in the transversely isotropic matrix for $\theta = 0^\circ$. Panels (a) and (b) show the variation of the real and imaginary wave numbers with the reduced frequency. For frequency response functions in panel (c), the blue solid, blue dashed, and red solid lines represent the results for the excitation of $(\bar{u}_x, \bar{u}_z, \bar{p})$, respectively.

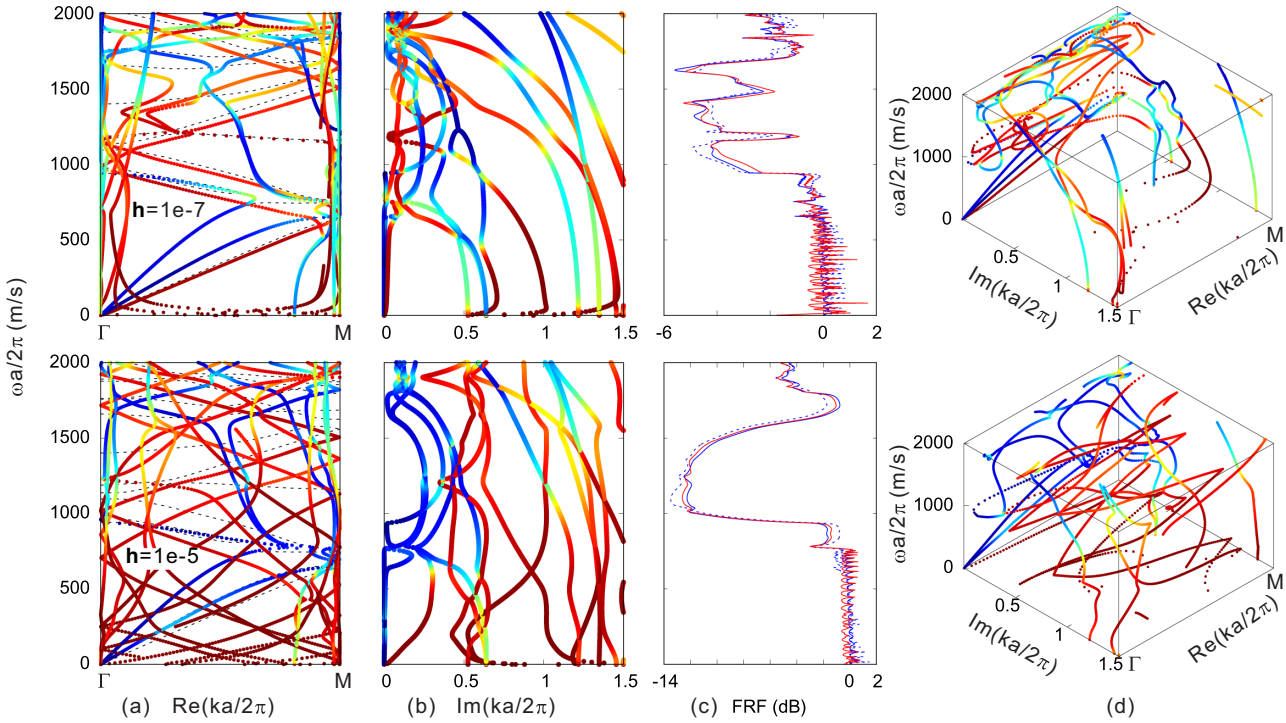

FIG. 7. Effects of fluid viscosity on the complex band structures and transmission spectrum of 2D periodic FSPMs in a transversely isotropic matrix for $\theta = 45^\circ$. Panels (a) and (b) show the variation of the real and imaginary wave numbers with the reduced frequency. For frequency response functions in panel (c), the blue solid, blue dashed, and red solid lines represent the results for the excitation of $(\bar{u}_x, \bar{u}_z, \bar{p})$, respectively.

gaps appear due to the interference of waves with different polarizations. These wave-number band gaps are continuously traversed by complex-frequency bands (supporting temporally damped waves), in striking opposition to frequency band gaps that are continuously traversed by complex-wave-number bands (supporting evanescent waves). It is further observed that material anisotropy can affect the complex band structures and the transmission curves. In particular, the existence of a QSV wave restricts the appearance of band gaps, and only directional band gaps appear in the 2D lossless FSPMs. When viscosity is introduced, all bands in the complex band structure move into the complex-wave-number space, and complete attenuation band gaps come up. The frequency response or transmission is then strongly dependent on the value of the viscosity of the fluid filling the pores but also on the direction of propagation.

The present paper was limited to metamaterials composed of FSP media only and could be extended to cases where FSP and elastic media are mixed or FSP media and fluids. Considering, in a similar light, the case of metamaterials with defects or in the gradient form would also be interesting. Such considerations could be of practical importance for novel FSPMs applied in the fields of civil engineering, geology, porous materials, and biology [49].

ACKNOWLEDGMENTS

Financial support by the National Natural Science Foundation of China (Grants No. 11702017, No. 11991032, and No. 11532001), the Young Elite Scientists Sponsorship Program by CAST (Grant No. YESS20170022), and the EIPHI Graduate School (Grant No. ANR-17-EURE-0002) are gratefully acknowledged.

APPENDIX A: BASIC EQUATIONS FROM BIOT'S THEORY

Following Biot [9,10], the constitutive equations for wave propagation in transversely isotropic FSP media can be expressed as

$$\begin{aligned}
\tau_{xx} &= (2B_1 + B_2)e_{xx} + B_2 e_{yy} + B_3 e_{zz} + B_6\xi,\\
\tau_{yy} &= B_2 e_{xx} + (2B_1 + B_2)e_{yy} + B_3 e_{zz} + B_6\xi,\\
\tau_{zz} &= B_3 e_{xx} + B_3 e_{yy} + B_4 e_{zz} + B_7\xi,\\
\tau_{yz} &= 2B_5 e_{yz}, \quad \tau_{zx} = 2B_5 e_{zx}, \quad \tau_{xy} = 2B_1 e_{xy},\\
p &= B_6 e_{xx} + B_6 e_{yy} + B_7 e_{zz} + B_8\xi.
\end{aligned} \tag{A1}$$

In these expressions, τ_{ij} and $e_{ij}(i, j = x, y, z)$ are the stress and strain tensors of the solid skeleton, p is the pore fluid pressure, and ξ is the increment of the fluid content per unit volume. The displacement components of the skeleton and of the fluid are u_i and U_i. The strain e_{ij} and the increment ξ can be expressed as

$$e_{ij} = \tfrac{1}{2}(u_{i,j} + u_{j,i}), \quad \xi = -w_{i,i}, \tag{A2}$$

where $w_i = \phi(U_i - u_i)$ and ϕ is the porosity of the medium (a number between 0 and 1). The material coefficients B_1 to B_8 are determined by the material constants of the skeleton and of the fluid [38],

$$\begin{aligned}
&B_1 = C_{66}, \quad B_2 = C_{12} + B_6^2/B_8, \quad B_3 = C_{13} + B_6 B_7/B_8,\\
&B_4 = C_{33} + B_7^2/B_8, \quad B_5 = C_{44},\\
&B_6 = -\left(1 - \frac{C_{11} + C_{12} + C_{13}}{3K_s}\right)B_8,\\
&B_7 = -\left[1 - \frac{(2C_{13} + C_{33})}{3K_s}\right]B_8,\\
&B_8 = \left(\frac{1-\phi}{K_s} + \frac{\phi}{K_f} - \frac{2C_{11} + 2C_{12} + 4C_{13} + C_{33}}{9K_s^2}\right)^{-1},
\end{aligned} \tag{A3}$$

where C_{ij}'s are the homogenized elastic constants of the solid skeleton in Biot's theory, K_s is the microscopic bulk modulus of the solid material from which the skeleton is made [38], and K_f is the microscopic bulk modulus of the pore fluid.

The equations of motion can be written in Cartesian coordinates as

$$\tau_{ij,j} = \rho\ddot{u}_i + \rho_f\ddot{w}_i, \quad -p_{,i} = \rho_f\ddot{u}_i + m_{ii}\ddot{w}_i + r_{ii}\dot{w}_i, \tag{A4}$$

where $\rho = (1-\phi)\rho_s + \phi\rho_f$, ρ_f, and ρ_s are the mass densities of the FSP media, the solid skeleton, and the pore fluid, respectively. m_{ii} and r_{ii} are coefficients introduced by Biot. For transversely isotropic porous materials, we have $m_{11} = m_{22} = m_1$, $m_{33} = m_3$, $r_{11} = r_{22} = r_1$, and $r_{33} = r_3$.

For harmonic waves at angular frequency ω, the Biot coefficients m_i and r_i are functions of angular frequency ω and can be written [17,40]

$$m_i = \mathrm{Re}[\alpha_i(\omega)]\rho_f/\phi, \quad r_i = \mathrm{Re}[\eta/K_i(\omega)], \tag{A5}$$

where η is the viscosity of the fluid and $\alpha_i(\omega)$ and $K_i(\omega)$ are the dynamic tortuosity and permeability, respectively, with the relation,

$$\alpha_i(\omega) = \imath\eta\phi/[K_i(\omega)\omega\rho_f]. \tag{A6}$$

For porous media with pores of simple form, the dynamic permeability can be expressed asymptotically [50]

$$K_i(\omega) = K_i(0)\left(\left[1 - \frac{4\imath\alpha_i^2(\infty)K_i^2(0)\omega\rho_f}{\eta d_i^2\phi^2}\right]^{1/2} - \frac{\imath\alpha_i(\infty)K_i(0)\omega\rho_f}{\eta\phi}\right)^{-1}, \tag{A7}$$

where d_i is the characteristic length of the pores. When the pores are a set of nonintersecting tubes, we further have $8\alpha_i(\infty)K_i(0)/(\phi d_i^2) = 1$.

APPENDIX B: COMPLEX-WAVE-NUMBER BAND STRUCTURE FOR LOSSY FSPMs

For a lossy metamaterial, we can obtain complex-wave-number band structures by using Eq. (7) with the following nonzero coefficient matrices that depend only on frequency

and on the propagation direction,

$$
\begin{aligned}
A_0 &= -\begin{bmatrix} \begin{pmatrix} B_9 & 0 \\ 0 & B_5 \end{pmatrix} & \begin{pmatrix} 0 & (B_{10}-B_5) \\ B_5 & 0 \end{pmatrix} & \begin{pmatrix} 0 & 0 \\ 0 & 0 \end{pmatrix} \\ \begin{pmatrix} 0 & B_5 \\ (B_{10}-B_5) & 0 \end{pmatrix} & \begin{pmatrix} B_5 & 0 \\ 0 & \left(B_4-\frac{B_7^2}{B_8}\right) \end{pmatrix} & \begin{pmatrix} 0 & 0 \\ 0 & 0 \end{pmatrix} \\ \begin{pmatrix} 0 & 0 \\ 0 & 0 \end{pmatrix} & \begin{pmatrix} 0 & 0 \\ 0 & 0 \end{pmatrix} & \begin{pmatrix} \frac{-1}{m_1\omega^2} & 0 \\ 0 & \frac{-1}{m_3\omega^2} \end{pmatrix} \end{bmatrix}, \\
A_1 &= \begin{pmatrix} B_9 l_1^2 + B_5 l_3^2 & B_{10} l_1 l_3 & 0 \\ B_{10} l_1 l_3 & B_5 l_1^2 + \left(B_4 - \frac{B_7^2}{B_8}\right) l_3^2 & 0 \\ 0 & 0 & -\left(\frac{l_1^2}{m_1\omega^2} + \frac{l_3^2}{m_3\omega^2}\right) \end{pmatrix}, \\
A_2 &= -\begin{pmatrix} 0 & 0 & \left(\frac{B_6}{B_8} + \frac{\rho_f}{m_1}\right) l_1 \\ 0 & 0 & \left(\frac{B_7}{B_8} + \frac{\rho_f}{m_3}\right) l_3 \\ \left(\frac{B_6}{B_8} + \frac{\rho_f}{m_1}\right) l_1 & \left(\frac{B_7}{B_8} + \frac{\rho_f}{m_3}\right) l_3 & 0 \end{pmatrix}, \\
A_3 &= -\begin{bmatrix} \begin{pmatrix} B_9\lambda l_1 \\ B_5\lambda l_3 \end{pmatrix} & \begin{pmatrix} (B_{10}-B_5)\lambda l_3 \\ B_5\lambda l_1 \end{pmatrix} & \begin{pmatrix} 0 \\ 0 \end{pmatrix} \\ \begin{pmatrix} B_5\lambda l_3 \\ (B_{10}-B_5)\lambda l_1 \end{pmatrix} & \begin{pmatrix} B_5\lambda l_1 \\ \left(B_4-\frac{B_7^2}{B_8}\right)\lambda l_3 \end{pmatrix} & \begin{pmatrix} 0 \\ 0 \end{pmatrix} \\ \begin{pmatrix} 0 \\ 0 \end{pmatrix} & \begin{pmatrix} 0 \\ 0 \end{pmatrix} & \begin{pmatrix} \frac{-\lambda l_1}{m_1\omega^2} \\ \frac{-\lambda l_3}{m_3\omega^2} \end{pmatrix} \end{bmatrix}, \\
A_4 &= \begin{bmatrix} (B_9\lambda l_1 & B_5\lambda l_3) & (B_5\lambda l_3 & (B_{10}-B_5)\lambda l_1) & \left(\frac{B_6}{B_8}+\frac{\rho_f}{m_1} & 0\right) \\ ((B_{10}-B_5)\lambda l_3 & B_5\lambda l_1) & \left[B_5\lambda l_1 & \left(B_4-\frac{B_7^2}{B_8}\right)\lambda l_3\right] & \left(0 & \frac{B_7}{B_8}+\frac{\rho_f}{m_3}\right) \\ \left(\frac{B_6}{B_8}+\frac{\rho_f}{m_1} & 0\right) & \left(0 & \frac{B_7}{B_8}+\frac{\rho_f}{m_3}\right) & \left(\frac{-\lambda l_1}{m_1\omega^2} & \frac{-\lambda l_3}{m_3\omega^2}\right) \end{bmatrix}, \\
A_5 &= \begin{pmatrix} \left(\rho - \frac{\rho_f^2}{m_1}\right)\omega^2 & 0 & 0 \\ 0 & \left(\rho - \frac{\rho_f^2}{m_3}\right)\omega^2 & 0 \\ 0 & 0 & \frac{-1}{B_8} \end{pmatrix}.
\end{aligned} \tag{B1}
$$

As a result, the generalized eigenvalue problem defined by those matrices is linear.

APPENDIX C: APPENDIX C: COMPLEX-FREQUENCY BAND STRUCTURE FOR LOSSLESS FSPMs

For a lossless metamaterial, we can obtain the complex-frequency band structures by using Eq. (7) with the following nonzero coefficient matrices:

$$
A_0 = -\begin{bmatrix} \begin{pmatrix} B_9 & 0 \\ 0 & B_5 \end{pmatrix} & \begin{pmatrix} 0 & (B_{10}-B_5) \\ B_5 & 0 \end{pmatrix} & \begin{pmatrix} 0 & 0 \\ 0 & 0 \end{pmatrix} \\ \begin{pmatrix} 0 & B_5 \\ (B_{10}-B_5) & 0 \end{pmatrix} & \begin{pmatrix} B_5 & 0 \\ 0 & \left(B_4-\frac{B_7^2}{B_8}\right) \end{pmatrix} & \begin{pmatrix} 0 & 0 \\ 0 & 0 \end{pmatrix} \\ \begin{pmatrix} 0 & 0 \\ 0 & 0 \end{pmatrix} & \begin{pmatrix} 0 & 0 \\ 0 & 0 \end{pmatrix} & \begin{pmatrix} \frac{-1}{m_1} & 0 \\ 0 & \frac{-1}{m_3} \end{pmatrix} \end{bmatrix},
$$

$$A_1 = -\begin{pmatrix} \left(\rho - \frac{\rho_f^2}{m_1}\right) & 0 & 0 \\ 0 & \left(\rho - \frac{\rho_f^2}{m_3}\right) & 0 \\ 0 & 0 & \frac{-1}{B_8} \end{pmatrix},$$

$$A_3 = -\begin{bmatrix} \begin{pmatrix} B_9 \imath k l_1 \\ B_5 \imath k l_3 \end{pmatrix} & \begin{pmatrix} (B_{10} - B_5) \imath k l_3 \\ B_5 \imath k l_1 \end{pmatrix} & \begin{pmatrix} 0 \\ 0 \end{pmatrix} \\ \begin{pmatrix} B_5 \imath k l_3 \\ (B_{10} - B_5) \imath k l_1 \end{pmatrix} & \begin{bmatrix} B_5 \imath k l_1 \\ \left(B_4 - \frac{B_7^2}{B_8}\right) \imath k l_3 \end{bmatrix} & \begin{pmatrix} 0 \\ 0 \end{pmatrix} \\ \begin{pmatrix} 0 \\ 0 \end{pmatrix} & \begin{pmatrix} 0 \\ 0 \end{pmatrix} & \begin{pmatrix} -\frac{\imath k l_1}{m_1} \\ -\frac{\imath k l_3}{m_3} \end{pmatrix} \end{bmatrix},$$

$$A_4 = \begin{bmatrix} (B_9 \imath k l_1 \quad B_5 \imath k l_3) & (B_5 \imath k l_3 \quad (B_{10} - B_5) \imath k l_1) & \left(\frac{B_6}{B_8} + \frac{\rho_f}{m_1} \quad 0\right) \\ ((B_{10} - B_5) \imath k l_3 \quad B_5 \imath k l_1) & \begin{bmatrix} B_5 \imath k l_1 & \left(B_4 - \frac{B_7^2}{B_8}\right) \imath k l_3 \end{bmatrix} & \left(0 \quad \frac{B_7}{B_8,} + \frac{\rho_f}{m_3}\right) \\ \left[-\left(\frac{B_6}{B_8} + \frac{\rho_f}{m_1}\right)\lambda^2 \quad 0\right] & \left[0 \quad -\left(\frac{B_7}{B_8} + \frac{\rho_f}{m_3}\right)\lambda^2\right] & \left(-\frac{\imath k l_1}{m_1} \quad -\frac{\imath k l_3}{m_3}\right) \end{bmatrix},$$

$$A_5 = -\begin{pmatrix} B_9 k^2 l_1^2 + B_5 k^2 l_3^2 & B_{10} k^2 l_1 l_3 & -\left(\frac{B_6}{B_8} + \frac{\rho_f}{m_1}\right) \imath k l_1 \\ B_{10} k^2 l_1 l_3 & B_5 k^2 l_1^2 - \left(B_4 - \frac{B_7^2}{B_8}\right) k^2 l_3^2 & -\left(\frac{B_7}{B_8} + \frac{\rho_f}{m_3}\right) \imath k l_3 \\ \left(\frac{B_6}{B_8} + \frac{\rho_f}{m_1}\right) \imath \lambda^2 k l_1 & \left(\frac{B_7}{B_8} + \frac{\rho_f}{m_3}\right) \imath \lambda^2 k l_3 & -\left(\frac{k^2 l_1^2}{m_1} + \frac{k^2 l_3^2}{m_3}\right) \end{pmatrix}. \tag{C1}$$

Those matrices depend on the wave number, on the propagation direction, but also on the frequency eigenvalue itself. The generalized eigenvalue problem is, thus, nonlinear. In the absence of a particular symmetry, the appearance of complex eigenfrequencies is permitted.

APPENDIX D: FREQUENCY RESPONSE FUNCTION FOR A FINITE FSPM

For a finite FSPM, we can obtain the FRF by using Eq. (7) with the same matrix A_0 as that in Eq. (B1), but

$$A_3 = \begin{bmatrix} \begin{pmatrix} 0 \\ 0 \end{pmatrix} & \begin{pmatrix} 0 \\ 0 \end{pmatrix} & \begin{pmatrix} \frac{B_6}{B_8} + \frac{\rho_f}{m_1} \\ 0 \end{pmatrix} \\ \begin{pmatrix} 0 \\ 0 \end{pmatrix} & \begin{pmatrix} 0 \\ 0 \end{pmatrix} & \begin{pmatrix} 0 \\ \frac{B_7}{B_8} + \frac{\rho_f}{m_3} \end{pmatrix} \\ \begin{pmatrix} \frac{B_6}{B_8} + \frac{\rho_f}{m_1} \\ 0 \end{pmatrix} & \begin{pmatrix} 0 \\ \frac{B_7}{B_8} + \frac{\rho_f}{m_3} \end{pmatrix} & \begin{pmatrix} 0 \\ 0 \end{pmatrix} \end{bmatrix}, \tag{D1}$$

$$A_5 = \begin{pmatrix} \left(\rho - \frac{\rho_f^2}{m_1}\right)\omega^2 & 0 & 0 \\ 0 & \left(\rho - \frac{\rho_f^2}{m_3}\right)\omega^2 & 0 \\ 0 & 0 & \frac{-1}{B_8} \end{pmatrix}. \tag{D2}$$

Other matrices are zero.

APPENDIX E: DISPERSION RELATION FOR HOMOGENEOUS FSP MEDIA

The coefficients in Eq. (E1) are

$$\begin{aligned} b = {} & \left[(B_3 + 2B_5)B_3B_8^2 - (2B_1 + B_2)B_4B_8^2 + (2B_1 + B_2)B_7^2B_8 + B_4B_6^2B_8 - 2(B_3 + B_5)B_6B_7B_8\right]\left(m_1 l_3^2 + m_3 l_1^2\right) l_1^2 l_3^2 m_1 m_3 \\ & + \left(B_7^2 - B_4B_8\right)B_5B_8\left(m_1 l_3^2 + m_3 l_1^2\right) l_3^4 m_1 m_3 + \left[B_6^2 - (2B_1 + B_2)B_8\right]B_5B_8\left(m_1 l_3^2 + m_3 l_1^2\right) l_1^4 m_1 m_3, \\ c = {} & \left\{(2B_1 + B_2)B_5B_8 m_1 m_3 + \left[(2B_1 + B_2 + B_5)B_8^2\rho + (2B_5\rho_f - B_6\rho)B_6B_8\right]m_3 + \left(B_6^2 - 2B_1B_8 - B_2B_8\right)\right. \\ & \left. \times\ B_8\rho_f^2\right\} l_1^4 m_1 m_3 + \left[B_4B_5B_8 m_1 m_3 + \left(B_4B_8^2\rho + B_5B_8^2\rho - B_7^2B_8\rho + 2B_5B_7B_8\rho_f\right)m_1 + \left(B_7^2 - B_4B_8\right)B_8\rho_f^2\right] l_3^4 m_1 m_3 \\ & + \left[\left(2B_1B_4B_8 + B_2B_4B_8 - B_3^2B_8 - 2B_3B_5B_8\right)m_1 m_3 + \left(2B_1B_8^2\rho + B_2B_8^2\rho + B_5B_8^2\rho - B_6^2B_8\rho + 4B_1B_7B_8\rho_f\right.\right. \end{aligned}$$

$$
\begin{aligned}
&+ 2B_2B_7B_8\rho_f - 2B_3B_6B_8\rho_f - 2B_5B_6B_8\rho_f\big)m_1 + \big(B_4B_8^2\rho + B_5B_8^2\rho - B_7^2B_8\rho - 2B_3B_7B_8\rho_f + 2B_4B_6B_8\rho_f \\
&- 2B_5B_7B_8\rho_f\big)m_3 + \big(2B_6B_7 - 2B_3B_8 - 4B_5B_8\big)B_8\rho_f^2\big]l_1^2l_3^2m_1m_3, \\
d =& \big[\big(B_5B_8\rho_f^2 - B_8^2\rho^2 + 2B_6B_8\rho\rho_f\big)m_3 - (2B_1 + B_2 + B_5)B_8\rho m_1m_3 + (2B_1 + B_2)B_8\rho_f^2m_1 + (B_8\rho + 2B_6\rho_f) \\
&\times B_8\rho_f^2\big]m_1m_3l_1^2 + \big[\big(B_8^2\rho^2 - B_5B_8\rho_f^2 + 2B_7B_8\rho\rho_f\big)m_1 + (B_4 + B_5)B_8\rho m_1m_3 - B_4B_8\rho_f^2m_3 \\
&- \big(B_8\rho + 2B_7\rho_f\big)B_8\rho_f^2\big]m_1m_3l_3^2, \\
e =& B_8m_1m_3\big(\rho m_1 - \rho_f^2\big)\big(\rho m_3 - \rho_f^2\big).
\end{aligned} \tag{E1}
$$

[1] M. I. Hussein, M. J. Leamy, and M. Ruzzene, Appl. Mech. Rev. **66**, 040802 (2014).
[2] M. S. Kushwaha, P. Halevi, L. Dobrzynski, and B. Djafari-Rouhani, Phys. Rev. Lett. **71**, 2022 (1993).
[3] Z. Liu, X. Zhang, Y. Mao, Y. Y. Zhu, Z. Yang, C. T. Chan, and P. Sheng, Science **289**, 1734 (2000).
[4] Z. Liu, C. T. Chan, and P. Sheng, Phys. Rev. B **71**, 014103 (2005).
[5] Y.-F. Wang, Y.-S. Wang, and V. Laude, Phys. Rev. B **92**, 104110 (2015).
[6] G. Ma and P. Sheng, Sci. Adv. **2**, e1501595 (2016).
[7] V. Laude, *Phononic Crystals: Artificial Crystals for Sonic, Acoustic, and Elastic Waves* (de Gruyter GmbH, Berlin, 2015).
[8] Y.-F. Wang, Y.-Z. Wang, B. Wu, W. Chen, and Y.-S. Wang, Appl. Mech. Rev. **72**, 040801 (2020).
[9] M. A. Biot, J. Acoust. Soc. Am. **28**, 168 (1956).
[10] M. A. Biot, J. Acoust. Soc. Am. **28**, 179 (1956).
[11] H. Deresiewicz, Bull. Seismol. Soc. Am. **52**, 627 (1962).
[12] B. R. Simon, O. C. Zienkiewicz, and D. K. Paul, Int. J. Numer. Anal. Methods Geomech. **8**, 381 (1984).
[13] A. Nur, *Wave Propagation in the Two-Phase Media* (Petroleum Industry Press, Beijing, 1986).
[14] T. J. Plona, Appl. Phys. Lett. **36**, 259 (1980).
[15] N. C. Dutta, Appl. Phys. Lett. **37**, 898 (1980).
[16] L. Xiong, B. Nennig, Y. Auregan, and W. Bi, J. Acoust. Soc. Am. **142**, 2288 (2017).
[17] R. D. Stoll and G. M. Bryan, J. Acoust. Soc. Am. **47**, 1440 (1970).
[18] L. De Ryck, J. P. Groby, P. Leclaire, W. Lauriks, A. Wirgin, Z. E. A. Fellah, and C. Depollier, Appl. Phys. Lett. **90**, 181901 (2007).
[19] Y. Liu and L. T. Gao, Int. J. Solids Struct. **45**, 4860 (2008).
[20] S. C. Cowin and L. Cardoso, J. Biomech. **48**, 842 (2015).
[21] A. Pooladi, M. Rahimian, and R. Y. S. Pak, Appl. Math. Modell. **50**, 177 (2017).
[22] K. A. Kuo and H. E. M. Hunt, Appl. Mech. Rev. **65**, 031003 (2013).
[23] G. Finocchio, O. Casablanca, G. Ricciardi, U. Alibrandi, F. Garesci, M. Chiappina, and B. Azzerboni, Appl. Phys. Lett. **104**, 191903 (2014).
[24] D. J. Colquitt, A. Colombi, R. V. Craster, P. Roux, and S. R. L. Guenneau, J. Mech. Phys. Solids **99**, 379 (2017).
[25] Y. Achaoui, T. Antonakakis, S. Brûlé, R. V. Craster, S. Enoch, and S. Guenneau, New J. Phys. **19**, 063022 (2017).
[26] Muhammad, C. K. Lim, and J. N. Reddy, Eng. Struct. **188**, 440 (2019).
[27] S. Brûlé, E. H. Javelaud, S. Enoch, and S. Guenneau, Phys. Rev. Lett. **112**, 133901 (2014).
[28] Y. Yan, A. Laskar, Z. Cheng, F. Meng, Y. Tang, Y. L. Mo, and Z. F. Shi, J. Appl. Phys. **116**, 044908 (2014).
[29] A. Colombi, P. Roux, S. Guenneau, P. Gueguen, and R. V. Craster, Sci. Rep. **6**, 19238 (2016).
[30] J.-P. Groby, O. Dazel, A. Duclos, L. Boeckx, and L. Kelders, J. Acoust. Soc. Am. **130**, 3771 (2011).
[31] J. Yang, J. S. Lee, and Y. Y. Kim, J. Phys. D: Appl. Phys. **50**, 015301 (2017).
[32] T. Weisser, J.-P. Groby, O. Dazel, F. Gaultier, E. Deckers, S. Futatsugi, and L. Monteiro, J. Acoust. Soc. Am. **139**, 617 (2016).
[33] H. Franklin, F. Luppé, and J. M. Conoir, J. Acoust. Soc. Am. **135**, 2513 (2014).
[34] A. Alevizaki, R. Sainidou, P. Rembert, B. Morvan, and N. Stefanou, Phys. Rev. B **94**, 174306 (2016).
[35] A. Alevizaki, R. Sainidou, P. Rembert, B. Morvan, and N. Stefanou, Phys. Rev. B **95**, 214306 (2017).
[36] W. Trabelsi, H. Franklin, A. Tinel, and S. Derible, Ultrasonics **54**, 1097 (2014).
[37] Y.-F. Wang, J.-W. Liang, A.-L. Chen, Y.-S. Wang, and V. Laude, Phys. Rev. B **99**, 134304 (2019).
[38] M. N. Kazi-Aoual, G. Bonnet, and P. Jouanna, J. Acoust. Soc. Am. **84**, 1883 (1988).
[39] J. M. Carcione, J. Acoust. Soc. Am. **99**, 2655 (1996).
[40] Y. S. Wang and Z. M. Zhang, J. Acoust. Soc. Am. **103**, 695 (1998).
[41] J. F. Allard and N. Atalla, *Propagation of Sound in Porous Media: Modeling Sound Absorbing Materials*, 2nd ed. (Wiley, Chichester, UK, 2009).
[42] P. N. J. Rasolofosaon, Appl. Phys. Lett. **52**, 780 (1988).
[43] V. Laude, Y. Achaoui, S. Benchabane, and A. Khelif, Phys. Rev. B **80**, 092301 (2009).
[44] J. S. Jensen, J. Sound Vib. **266**, 1053 (2003).
[45] Y. Liu, K. Liu, and S. Tanimura, JSME Int. J., Ser. A **45**, 348 (2002).
[46] M. I. Hussein and M. J. Frazier, J. Appl. Phys. **108**, 093506 (2010).
[47] T. T. Wang, V. Laude, M. Kadic, Y. F. Wang, and Y. S. Wang, Appl. Sci. **9**, 2825 (2019).
[48] R. P. Moiseyenko and V. Laude, Phys. Rev. B **83**, 064301 (2011).
[49] E. Rohan, S. Naili, R. Cimrman, and T. Lemaire, J. Mech. Phys. Solids **60**, 857 (2012).
[50] D. L. Johnson, J. Koplik, and R. Dashen, J. Fluid Mech. **176**, 379 (1987).